

CONTINUAL SELF-SUPERVISED LEARNING CONSIDERING MEDICAL DOMAIN KNOWLEDGE IN CHEST CT IMAGES

*Ren Tasai Guang Li Ren Togo Minghui Tang Takaaki Yoshimura Hiroyuki Sugimori
Kenji Hirata Takahiro Ogawa Kohsuke Kudo Miki Haseyama*

Hokkaido University

ABSTRACT

We propose a novel continual self-supervised learning method (CSSL) considering medical domain knowledge in chest CT images. Our approach addresses the challenge of sequential learning by effectively capturing the relationship between previously learned knowledge and new information at different stages. By incorporating an enhanced DER into CSSL and maintaining both diversity and representativeness within the rehearsal buffer of DER, the risk of data interference during pretraining is reduced, enabling the model to learn more richer and robust feature representations. In addition, we incorporate a mixup strategy and feature distillation to further enhance the model’s ability to learn meaningful representations. We validate our method using chest CT images obtained under two different imaging conditions, demonstrating superior performance compared to state-of-the-art methods.

Index Terms— Self-supervised learning, continual learning, mixup strategy, feature distillation, chest CT image.

1. INTRODUCTION

Self-supervised learning (SSL) has gained significant attention for its ability to reduce the annotation costs of large-scale datasets [1]. SSL methods typically involve two phases: pretraining and fine-tuning. During pretraining, a model learns feature representations directly from unlabeled data. In the fine-tuning stage, these learned representations are refined using a smaller labeled dataset [2, 3]. For large-scale medical datasets, annotations require expertise from physicians, which is both time-consuming and labor-intensive [4, 5]. As a result, there has been active research into medical SSL methods that work with limited labeled data from various modalities such as X-rays [6, 7], computed tomography (CT) [8, 9], and magnetic resonance imaging (MRI) [10, 11]. These studies have shown promising results of SSL for medical image analysis.

In the medical field, a variety of imaging modalities, including X-rays, CT, and MRI, are utilized. Due to the inherent dimensional differences between these modalities, such as 2D for X-rays and 3D for CT and MRI, recent researchers have explored SSL methods that pretrain across multiple modalities, simultaneously [12, 13]. However, these studies have reported no significant improvement in classification accuracy when pretraining involves multiple modalities [14], primarily due to insufficient handling of the distinct data

distributions, which causes interference during the pretraining process.

Recently, continual self-supervised learning (CSSL) [14] has been introduced to address data interference across modalities by considering differences in data distribution. CSSL preserves the diversity of data distribution during pretraining, allowing the model to maintain rich feature representations for later fine-tuning. A major challenge in CSSL, is catastrophic forgetting, where new knowledge overwrites previously learned information [15]. To address this problem, a rehearsal-based approach from continual learning is employed. This approach stores a portion of past data and features in a rehearsal buffer, enabling the model to retain and revisit prior knowledge during subsequent learning [16, 17]. Among these approaches, dark experience replay (DER) [16] is particularly effective in mitigating catastrophic forgetting during continual pretraining on diverse modalities.

Medical imaging relies on various domain-specific images depending on the equipment and imaging conditions [18, 19]. As a result, several researches have focused on medical SSL methods that can pretrain on multiple domains simultaneously [20, 21]. These domains capture the same anatomical region, whereas the modalities capture different anatomical regions. Therefore, these domains tend to have more similar data distributions compared to different modalities. However, prior studies often overlook differences in data distribution across domains, leading to data interference. In CSSL across multiple domains, it is crucial to maintain not only the diversity of data distributions but also their representativeness. To address this issue, we focus on capturing the relationship between past knowledge from earlier stages and future knowledge from subsequent stages.

This paper proposes a novel CSSL method that leverages medical domain knowledge in chest CT images. Specifically, our method incorporates an enhanced DER that ensures both diversity and representativeness in the rehearsal buffer by accounting for differences in data distributions across sequential learning stages. The enhanced DER allows us to minimize data interference during pretraining and enables the model to learn richer feature representations across multiple domains. Additionally, we integrate a mixup strategy and feature distillation to further improve representation learning. We pretrain using chest CT images obtained under two different imaging conditions and conduct evaluation on another open CT image dataset. Through extensive experiments, our method consistently outperforms other approaches.

Our contributions are summarized as follows.

- We propose a novel CSSL method that effectively addresses data distribution shifts during pretraining in chest CT images across two domains.
- By incorporating an enhanced DER into the CSSL method, it prevents data interference caused by the impact of differ-

This work was partly supported by JSPS KAKENHI Grant Numbers JP24K02942, JP23K21676, JP23K11141, and JP24K23849. We would like to thank the departments of radiology that provided the J-MID database, including Juntendo Univ., Kyushu Univ., Keio Univ., The Univ. of Tokyo, Okayama Univ., Kyoto Univ., Osaka Univ., Tokyo Medical and Dental Univ., Hokkaido Univ., Ehime Univ., and Tokushima Univ.

ent data distributions, enabling the model to acquire rich and robust feature representations.

- Extensive experiments show that our method outperforms state-of-the-art approaches on an open CT image dataset.

2. CONTINUAL SELF-SUPERVISED LEARNING METHOD CONSIDERING MEDICAL DOMAIN KNOWLEDGE

The proposed method employs a three-stage CSSL approach to mitigate catastrophic forgetting and reduce data interference between two domains in chest CT images. In the first stage, self-supervised learning is performed using the initial dataset D_1 from one domain of chest CT images. In the second stage, selected images from D_1 are stored in the rehearsal buffer, ensuring that both diversity and representativeness are maintained. In the third stage, continual self-supervised learning is applied using the next dataset D_2 from another domain and the obtained rehearsal buffer. After completing the CSSL process, the model is fine-tuned with labeled data for downstream tasks, such as classification. Figure 1 shows an overview of the proposed method.

2.1. Stage 1: Self-supervised Learning on Dataset D_1

The first stage of pretraining begins with training model M_1 using the first domain dataset D_1 . The Masked Autoencoders (MAE) method [22] based on masked image modeling is used to learn the input data’s feature representations. In this process, each image with C channels is divided into n patches of resolution (V, V) , and using a masking rate r , a subset of $m = n \times r$ patches is randomly masked. The $n - m$ unmasked patches are converted into token sequences by the tokenizer \mathcal{T}_{M_1} and are passed through the encoder ϕ_{M_1} to generate feature representations. The decoder ψ_{M_1} then reconstructs the masked patches based on these representations and the embeddings of the masked patches from the original image. The model is trained to minimize the mean squared error (MSE) between the original masked patches X_m and the reconstructed patches Y_m as follows:

$$\mathcal{L}_{\text{MSE}} = \frac{1}{m \times V^2 \times C} \|Y_m - X_m\|_2^2. \quad (1)$$

At the end of the first stage, the model M_1 is trained, capturing the rich feature representations of the first domain dataset D_1 . This trained model will also be used for the third stage of CSSL, which involves both D_1 and the second domain dataset D_2 .

2.2. Stage 2: Storing Image Samples in Rehearsal Buffer

The second stage involves the selection of images stored in the rehearsal buffer, which plays a critical role in capturing shifts in data distribution between stages, helping to mitigate catastrophic forgetting. In the second stage, we propose an enhanced DER that uses k -means sampling to account for the distributions of the domain datasets D_1 and D_2 , ensuring that the stored samples from D_1 are both diverse and representative. Figure 2 provides an overview illustration of this stage.

Let N_1 and N_2 represent the number of images in domain datasets D_1 and D_2 , respectively. Using the parameter α to determine the sampling ratio, the number of clusters is set to $K = N_1 \times \alpha$. The dataset D_1 is first clustered into K classes based on embeddings generated by the pretrained model M_1 , with each cluster denoted as \mathbf{a}_i , where $i \in \{1, 2, \dots, K\}$, and the feature vector of each cluster center represented as \mathbf{p}_i . The combined dataset of D_1 and

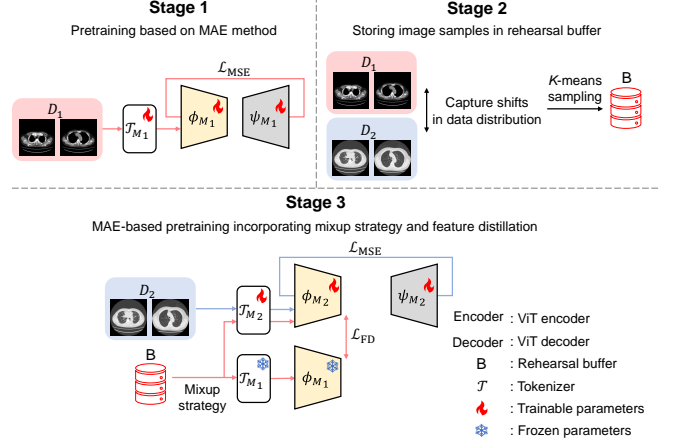


Fig. 1. Overview of the proposed CSSL method.

D_2 is then clustered into two classes, and the feature vector of the cluster center corresponding to dataset D_2 is denoted as \mathbf{q} . Next, the Euclidean distance L_i from each cluster center \mathbf{p}_i to \mathbf{q} is computed to evaluate how close each cluster of D_1 is to the class center of D_2 :

$$L_i = \|\mathbf{p}_i - \mathbf{q}\|_2. \quad (2)$$

Based on these distances, clusters \mathbf{a}_i are sorted in ascending order and divided into three groups: \mathbf{G}_1 , \mathbf{G}_2 , and \mathbf{G}_3 . Image samples are selected from each group according to the parameters γ_1 , γ_2 , and γ_3 , which determine the ratio of images retrieved from each group. Using the parameter β to determine the sampling ratio, the number of images stored in the rehearsal buffer B is set to $T = N_1 \times \beta$. These samples, $T \times \gamma_1$, $T \times \gamma_2$, and $T \times \gamma_3$ are selected from the points closest to the center of each respective cluster \mathbf{a}_i . The T image samples x_j , where $j \in \{1, 2, \dots, T\}$, are stored in the rehearsal buffer $B = \{x_j \mid x_j \in D_1\}$. The enhanced DER ensures that the rehearsal buffer B used for the third stage of CSSL retains diverse and representative image samples, effectively capturing the data distributions from both D_1 and D_2 .

2.3. Stage 3: Continual Self-supervised Learning on Dataset D_2

Following the SSL pretraining of model M_1 in the first stage, model M_2 is also pretrained in the third stage using the MAE method. In this stage, model M_2 is trained using both the second domain dataset D_2 and the image samples stored in the rehearsal buffer B that obtained from the second stage. We incorporate two critical techniques in this stage: the mixup strategy and feature distillation, both designed to enhance the model’s ability to retain knowledge from the first stage while learning new representations from the second domain.

The mixup strategy is applied to augment the image samples stored in the rehearsal buffer B , further improving the diversity of the data used for training. Let S denote the batch size, C the number of image channels, and (H, W) the image resolution. A batch of images $\mathbf{b} \in \mathbb{R}^{S \times C \times H \times W}$ is drawn from B , duplicated, and shuffled to create a new batch \mathbf{b}' . The mixed batch \mathbf{b}^{mix} is calculated as follows:

$$\mathbf{b}^{\text{mix}} = \lambda \odot \mathbf{b} + (1 - \lambda) \odot \mathbf{b}'. \quad (3)$$

Here, $\lambda \in \mathbb{R}^{S \times C \times H \times W}$ is a mask, where each element takes a random value in the range $[0, 1)$, determining the extent to which

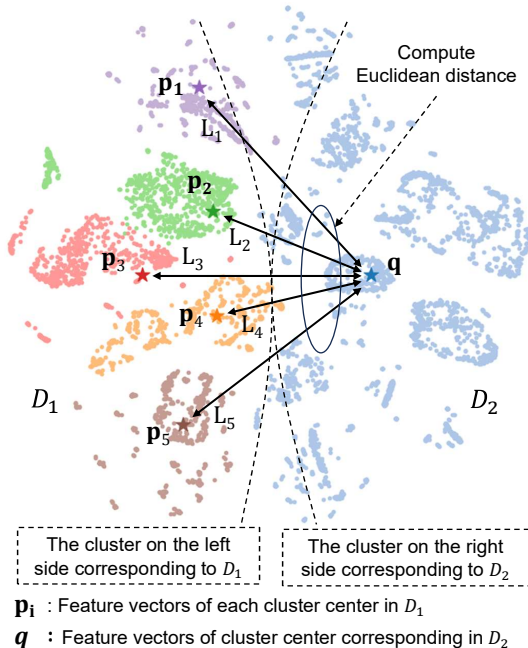


Fig. 2. Overview illustration of stage 2.

each sample in \mathbf{b} is mixed with the corresponding sample in \mathbf{b}' . This mixed batch \mathbf{b}^{mix} is then used to train model M_2 , improving the representation learning process in the third stage.

To further ensure that model M_2 retains knowledge from the first stage, feature distillation is employed. Specifically, the feature representations learned by M_1 are compared to those generated by M_2 during the third stage. The second domain dataset D_2 is passed only to M_2 , while the samples from the rehearsal buffer B are passed through both models. In this process, the mixed batch \mathbf{b}^{mix} are converted into token sequences by the tokenizers \mathcal{T}_{M_1} and \mathcal{T}_{M_2} and then passed through the encoders ϕ_{M_1} and ϕ_{M_2} , respectively. The following feature distillation loss \mathcal{L}_{FD} is calculated between the feature representations produced by M_1 and M_2 , ensuring that M_2 does not deviate significantly from the feature representations learned in the first stage:

$$\mathcal{L}_{\text{FD}} = \|\phi_{M_2}(\mathbf{b}^{\text{mix}}) - \text{StopGrad}(\phi_{M_1}(\mathbf{b}^{\text{mix}}))\|_2^2, \quad (4)$$

where $\phi_{M_1}(\mathbf{b}^{\text{mix}})$ represents the feature representation of \mathbf{b}^{mix} generated by the encoder ϕ_{M_1} from the first stage. $\phi_{M_2}(\mathbf{b}^{\text{mix}})$ is the feature representation of \mathbf{b}^{mix} produced by the encoder ϕ_{M_2} during the third stage. StopGrad is applied to $\phi_{M_1}(\mathbf{b}^{\text{mix}})$ to ensure that no gradient flows back through M_1 , keeping its parameters frozen during the training of M_2 . This feature distillation process helps model M_2 adapt to the new domain while preserving key knowledge from the first stage, ensuring better generalization across both domains, and balancing the knowledge from D_1 and D_2 . Algorithm 1 summarizes the proposed CSSL method.

By integrating an enhanced DER with a rehearsal-based strategy into the CSSL framework, the ViT encoder can efficiently capture the relationship between newly acquired data and previously learned knowledge across various medical domains. This approach minimizes data interference during pretraining and facilitates the learning of richer, more robust feature representations. Following the three-stage CSSL process, the pretrained ViT encoder can be fine-tuned on

Algorithm 1 Algorithm of the proposed CSSL method

Require: $\{D_1, D_2\}$: two datasets with different domains, B : rehearsal buffer, $\mathcal{T}_{M_1}, \mathcal{T}_{M_2}$: tokenizers, ϕ_{M_1}, ϕ_{M_2} : encoders, ψ_{M_1}, ψ_{M_2} : model-specific decoders, $\text{Sample}(\cdot)$: sampling operation

Ensure: $\phi_{M_2}, \mathcal{T}_{M_2}$

Stage 1:

- 1: Training dataset $D \leftarrow D_1$
- 2: Update $\phi_{M_1}, \mathcal{T}_{M_1}$, and ψ_{M_1} by \mathcal{L}_{MSE}
- 3: $B \leftarrow \text{Sample}(D_1)$

Stage 2:

- 4: Training dataset $D \leftarrow D_2 \cup B$
 - 5: **for** each interaction $i = 1$ to I **do**
 - 6: Sample a batch of unlabeled data x from D
 - 7: **if** $x \in D_2$ **then**
 - 8: Update $\phi_{M_2}, \mathcal{T}_{M_2}$, and ψ_{M_2} by \mathcal{L}_{MSE}
 - 9: **else**
 - 10: Update ϕ_{M_2} and \mathcal{T}_{M_2} by \mathcal{L}_{FD}
 - 11: **end if**
 - 12: **end for**
-

another labeled dataset for downstream tasks, such as classification.

3. EXPERIMENTS

3.1. Datasets and Settings

We constructed two subsets of chest CT images from the J-MID database¹ based on mediastinal and lung window settings, and used them as D_1 and D_2 for pretraining. The number of images N_1 and N_2 were 31,256 and 26,403, respectively. All of these images are grayscale and have a resolution of 512×512 pixels. For fine-tuning and evaluation, we trained the model using the SARS-CoV-2 CT-Scan Dataset [23] and validated it by performing a COVID-19 classification task. The SARS-CoV-2 CT-Scan Dataset contains a total of 2,481 chest CT images labeled into two classes: COVID-19 positive and negative. Out of these, 1,986 images were used for fine-tuning and 495 images were used for evaluation. In the pretraining of MAE, the masking ratio was set to $r = 0.75$, and the ViT-B [24] was used as the encoder. In each pretraining stage, a warm-up strategy was used during the first 40 epochs to gradually raise the learning rate from 0 to 0.00015, after which it was reduced to 0 in the following training using a cosine schedule. In k -means sampling, the parameters α and β , which determine the sampling ratio, were set to 0.01 and 0.05, respectively. Additionally, the number of clusters K and the number of samples T in the rehearsal buffer B were set to 312 and 1,562, respectively. The parameters γ_1, γ_2 , and γ_3 , which determine the number of images to be acquired, were set to 6, 3, and 1, respectively. The AdamW optimizer [25] was used in the fine-tuning phase, and the learning rate was set to 0.00005. We took SSL on the dataset for 300 epochs at each pretraining stage, followed by fine-tuning on the dataset for 80 epochs. As evaluation metrics, two-class classification accuracy (ACC), the area under the receiver operator curve (AUC), and F1 score (F1) were used.

The effectiveness of the learning order of domains in the proposed method was also verified by swapping D_1 and D_2 and conducting continual pretraining accordingly. Furthermore, to examine

¹<https://www.radiology.jp/j-mid/>

Table 1. Experimental results of the proposed method and comparative methods on the SARS-CoV-2 CT-Scan Dataset.

Method	Domain	ACC	AUC	F1
Ours	$D_1 \rightarrow D_2$	0.863	0.940	0.863
MedCoSS		0.836	0.923	0.836
Ours	$D_2 \rightarrow D_1$	0.800	0.900	0.798
MedCoSS		0.756	0.837	0.755
	$D_1 + D_2$	0.792	0.875	0.791
MAE	D_1	0.717	0.803	0.713
	D_2	0.756	0.817	0.755
Baseline	None	0.657	0.699	0.647

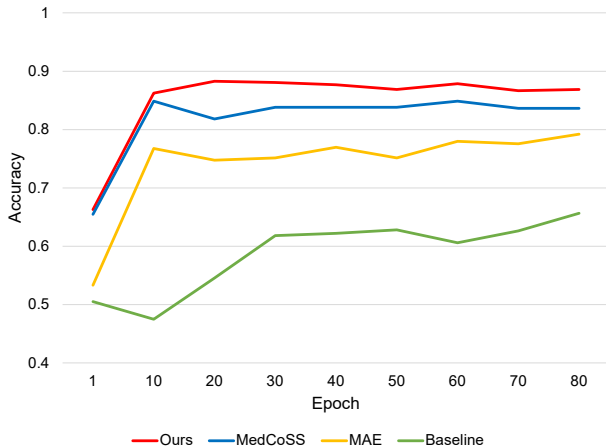


Fig. 3. Classification accuracy across different epochs during fine-tuning. All methods use ViT-B model.

how to consider the distance between data distributions of the two domains, we conducted an ablation study by varying the parameters γ_1 , γ_2 , and γ_3 , which determine the number of images to be acquired in the rehearsal buffer (see Subsec 3.3 for details).

To evaluate the effectiveness of the proposed method (Ours), we compared it against several approaches: MedCoSS [14], the state-of-the-art CSSL method, MAE [22] with simultaneous pretraining on both D_1 and D_2 , MAE pretrained only on D_1 , and MAE pretrained only on D_2 . As a baseline method, we used MAE fine-tuned without self-supervised pretraining.

3.2. Results and Discussion

From Table 1, we can observe that the proposed method outperforms all the comparative methods. From the three results of the MAE method, it was confirmed that pretraining with two domains improves accuracy compared to using a single domain. Additionally, as the proposed method outperforms the MAE method that simultaneously pretrains on two domains in evaluation metrics, it was confirmed that the proposed method can reduce data interference between domains compared to pretraining on multiple domains simultaneously. Furthermore, the experimental results show that when the model is pretrained on the domains in the same order, the proposed method outperforms MedCoSS in the evaluation metrics. This confirms that the proposed method, which takes data distribution between stages into account, is effective in reducing data interfer-

Table 2. Ablation study results of the proposed method on the SARS-CoV-2 CT-Scan Dataset. The best results are highlighted in bold, while the second-best are underlined.

Method	Domain	Ratio	ACC	AUC	F1
Ours	$D_1 \rightarrow D_2$	1:1:8	0.830	0.923	0.830
		1:3:6	0.820	0.928	0.819
		2:3:5	0.838	0.920	0.838
		<u>5:3:2</u>	<u>0.842</u>	<u>0.940</u>	<u>0.842</u>
		6:3:1	0.863	0.940	0.863
Ours	$D_2 \rightarrow D_1$	8:1:1	0.838	0.932	0.838
		1:1:8	0.669	0.712	0.668
		1:3:6	0.778	0.856	0.777
		2:3:5	0.756	0.838	0.755
		5:3:2	0.760	0.862	0.756
Ours	$D_2 \rightarrow D_1$	6:3:1	0.780	0.874	0.780
		8:1:1	0.800	0.900	0.798

ence. Furthermore, Fig. 3 shows that the proposed method achieves the fastest ACC convergence compared to all the comparative methods and consistently maintains the highest ACC at every number of epochs. This indicates that maintaining not only diversity but also representativeness of sample data within the rehearsal buffer can effectively reduce data interference between stages.

3.3. Ablation Studies

In the proposed method, we conducted an ablation study in which we varied the parameters γ_1 , γ_2 , and γ_3 , which determine the ratio of images acquired in the rehearsal buffer. This allows us to examine the optimal parameters that consider the differences in data distribution between stages to ensure diversity and representativeness within the rehearsal buffer. The ablation results are shown in Table 2. In the proposed method, which performs continual pretraining in the order from D_1 to D_2 , it is shown that the highest accuracy in the evaluation metrics is achieved when the parameters γ_1 , γ_2 , and γ_3 are set to 6, 3, and 1, respectively. Furthermore, it is observed that prioritizing the storage of samples that are closer in data distribution between domains in the rehearsal buffer, rather than those that are farther apart, tends to be more effective. It was confirmed that focusing on representativeness when storing samples in the rehearsal buffer is effective. This is likely because the domains capture the same anatomical regions, leading to similar data distributions and a tendency for the data distributions between domains to be closer. On the other hand, when γ_1 , γ_2 , and γ_3 are set to 8, 1, and 1, respectively, the accuracy in the evaluation metrics decreases. This suggests that it is preferable to maintain not only representativeness but also diversity.

4. CONCLUSION

In this paper, we presented a novel CSSL method that incorporates medical domain knowledge from chest CT images. By effectively capturing the differences in data distribution between two chest CT image domains and maintaining diversity and representativeness in the rehearsal buffer, our method enhances the representation learning process in CSSL. Additionally, we introduced a mixup strategy and feature distillation to further refine feature representations. Extensive experiments with chest CT images demonstrated that our approach outperforms state-of-the-art methods.

5. REFERENCES

- [1] Longlong Jing and Yingli Tian, “Self-supervised visual feature learning with deep neural networks: A survey,” *IEEE Transactions on Pattern Analysis and Machine Intelligence*, vol. 43, no. 11, pp. 4037–4058, 2020.
- [2] Guang Li, Ren Togo, Takahiro Ogawa, and Miki Haseyama, “Self-knowledge distillation based self-supervised learning for covid-19 detection from chest x-ray images,” in *Proceedings of the IEEE International Conference on Acoustics, Speech and Signal Processing (ICASSP)*, 2022, pp. 1371–1375.
- [3] Guang Li, Ren Togo, Takahiro Ogawa, and Miki Haseyama, “Self-supervised learning for gastritis detection with gastric x-ray images,” *International Journal of Computer Assisted Radiology and Surgery*, vol. 18, no. 10, pp. 1841–1848, 2023.
- [4] Alexander Chowdhury, Jacob Rosenthal, Jonathan Waring, and Renato Umeton, “Applying self-supervised learning to medicine: Review of the state of the art and medical implementations,” *Informatics*, vol. 8, no. 3, pp. 1–29, 2021.
- [5] Saeed Shurrah and Rehab Duwairi, “Self-supervised learning methods and applications in medical imaging analysis: A survey,” *PeerJ Computer Science*, vol. 8, pp. 1–51, 2022.
- [6] Guang Li, Ren Togo, Takahiro Ogawa, and Miki Haseyama, “Boosting automatic COVID-19 detection performance with self-supervised learning and batch knowledge ensembling,” *Computers in Biology and Medicine*, vol. 158, pp. 1–10, 2023.
- [7] Guang Li, Ren Togo, Takahiro Ogawa, and Miki Haseyama, “COVID-19 detection based on self-supervised transfer learning using chest x-ray images,” *International Journal of Computer Assisted Radiology and Surgery*, vol. 18, no. 4, pp. 715–722, 2022.
- [8] Yankai Jiang, Mingze Sun, Heng Guo, Xiaoyu Bai, Ke Yan, Le Lu, and Minfeng Xu, “Anatomical invariance modeling and semantic alignment for self-supervised learning in 3D medical image analysis,” in *Proceedings of the IEEE/CVF International Conference on Computer Vision (ICCV)*, 2023, pp. 15859–15869.
- [9] Chuyan Zhang, Hao Zheng, and Yun Gu, “Dive into the details of self-supervised learning for medical image analysis,” *Medical Image Analysis*, vol. 89, pp. 1–25, 2023.
- [10] Linxuan Han, Sa Xiao, Zimeng Li, Haidong Li, Xiuchao Zhao, Fumin Guo, Yeqing Han, and Xin Zhou, “Enhanced self-supervised learning for multi-modality MRI segmentation and classification: A novel approach avoiding model collapse,” *arXiv preprint arXiv:2407.10377*, 2024.
- [11] Aiham Taleb, Winfried Loetzsch, Noel Danz, Julius Severin, Thomas Gaertner, Benjamin Bergner, and Christoph Lippert, “3D self-supervised methods for medical imaging,” in *Proceedings of the Advances in Neural Information Processing Systems (NeurIPS)*, 2020, pp. 18158–18172.
- [12] Yutong Xie, Jianpeng Zhang, Yong Xia, and Qi Wu, “Unimiss: Universal medical self-supervised learning via breaking dimensionality barrier,” in *Proceedings of the European Conference on Computer Vision (ECCV)*, 2022, pp. 558–575.
- [13] Aiham Taleb, Christoph Lippert, Tassilo Klein, and Moin Nabi, “Multimodal self-supervised learning for medical image analysis,” in *Proceedings of Information Processing in Medical Imaging (IPMI)*, 2021, pp. 661–673.
- [14] Yiwen Ye, Yutong Xie, Jianpeng Zhang, Ziyang Chen, Qi Wu, and Yong Xia, “Continual self-supervised learning: Towards universal multi-modal medical data representation learning,” in *Proceedings of the IEEE/CVF Conference on Computer Vision and Pattern Recognition (CVPR)*, 2024, pp. 11114–11124.
- [15] Robert M. French, “Catastrophic interference in connectionist networks: Can it be predicted, can it be prevented?,” in *Proceedings of the Conference on Neural Information Processing Systems (NeurIPS)*, 1993, pp. 1176–1177.
- [16] Pietro Buzzega, Matteo Boschini, Angelo Porrello, Davide Abati, and Simone Calderara, “Dark experience for general continual learning: A strong, simple baseline,” in *Proceedings of the Advances in Neural Information Processing Systems (NeurIPS)*, 2020, pp. 15920–15930.
- [17] Matthew Riemer, Ignacio Cases, Robert Ajemian, Miao Liu, Irina Rish, Yuhai Tu, and Gerald Tesauro, “Learning to learn without forgetting by maximizing transfer and minimizing interference,” in *Proceedings of the International Conference on Learning Representations (ICLR)*, 2019, pp. 1–31.
- [18] Qiuli Wang, Xin Tan, Lizhuang Ma, and Chen Liu, “Dual windows are significant: Learning from mediastinal window and focusing on lung window,” in *Proceedings of Chinese Association for Artificial Intelligence (CICAI)*, 2022, pp. 191–203.
- [19] Hong Lu, Jongphil Kim, Jin Qi, Qian Li, Ying Liu, Matthew B Schabath, Zhaoxiang Ye, Robert J Gillies, and Yoganand Balagurunathan, “Multi-window ct based radiological traits for improving early detection in lung cancer screening,” *Cancer Management and Research*, pp. 12225–12238, 2020.
- [20] Hao Zheng, Jun Han, Hongxiao Wang, Lin Yang, Zhuo Zhao, Chaoli Wang, and Danny Z. Chen, “Hierarchical self-supervised learning for medical image segmentation based on multi-domain data aggregation,” in *Proceedings of the Medical Image Computing and Computer Assisted Intervention (MICCAI)*, 2021, pp. 622–632.
- [21] Ran Gu, Jingyang Zhang, Guotai Wang, Wenhui Lei, Tao Song, Xiaofan Zhang, Kang Li, and Shaoting Zhang, “Contrastive semi-supervised learning for domain adaptive segmentation across similar anatomical structures,” *IEEE Transactions on Medical Imaging*, vol. 42, no. 1, pp. 245–256, 2023.
- [22] Kaiming He, Xinlei Chen, Saining Xie, Yanghao Li, Piotr Dollár, and Ross Girshick, “Masked autoencoders are scalable vision learners,” in *Proceedings of the IEEE/CVF Conference on Computer Vision and Pattern Recognition (CVPR)*, 2022, pp. 16000–16009.
- [23] Eduardo Soares, Plamen Angelov, Sarah Biaso, Michele Higa Froes, and Daniel Kanda Abe, “SARS-CoV-2 CT-scan dataset: A large dataset of real patients CT scans for SARS-CoV-2 identification,” *MedRxiv*, 2020.
- [24] Alexey Dosovitskiy, Lucas Beyer, Alexander Kolesnikov, Dirk Weissenborn, Xiaohua Zhai, Thomas Unterthiner, Mostafa Dehghani, Matthias Minderer, Georg Heigold, Sylvain Gelly, Jakob Uszkoreit, and Neil Houlsby, “An image is worth 16x16 words: Transformers for image recognition at scale,” in *Proceedings of the International Conference on Learning Representations (ICLR)*, 2021, pp. 1–21.
- [25] Ilya Loshchilov and Frank Hutter, “Decoupled weight decay regularization,” in *Proceedings of the International Conference on Learning Representations (ICLR)*, 2019, pp. 1–18.